High-spin states and possible "stapler" band in ^{115}In

Z. Q. Chen (陈志强),[1] S. Y. Wang (王守宇),[1,*] L. Liu (刘雷),[1] P. Zhang (张盼),[1] H. Jia (贾慧),[1] B. Qi (亓斌),[1] S. Wang (王硕),[1] D. P. Sun (孙大鹏),[1] C. Liu (刘晨),[1] Z. Q. Li (李志泉),[1] X. G. Wu (吴晓光),[2] G. S. Li (李广生),[2] C. Y. He (贺创业),[2] Y. Zheng (郑云),[2] and L. H. Zhu (竺礼华)[3]

[1]*Shandong Provincial Key Laboratory of Optical Astronomy and Solar-Terrestrial Environment, Institute of Space Sciences, Shandong University, Weihai 264209, China*

[2]*China Institute of Atomic Energy, Beijing 102413, China*

[3]*School of Physics and Nuclear Energy Engineering, Beihang University, Beijing 100191, China*

(Received 21 December 2014; revised manuscript received 13 February 2015; published 7 April 2015)

High-spin states of ^{115}In have been studied using the ^{114}Cd (^{7}Li, α2n) reaction at a beam energy of 48 MeV. A total of 13 new transitions have been observed and added to the level scheme of ^{115}In. Most of the states in ^{115}In can be interpreted in terms of the weak coupling of a $g_{9/2}$ proton hole to the core states of ^{116}Sn or a $g_{7/2}$ proton to the core states of ^{114}Cd. A $\Delta I = 1$ band with the $\pi(g_{9/2})^{-1} \otimes \nu(h_{11/2})^2$ configuration was suggested as an oblate band built on the "stapler" mechanism with the aid of the tilted axis cranking model based on covariant density functional theory.

DOI: 10.1103/PhysRevC.91.044303 PACS number(s): 27.60.+j, 23.20.Lv, 21.10.Re, 21.60.Ev

I. INTRODUCTION

The level structures of excited states in nuclei near the $Z \sim 50$ region provide a wealth of information on the coexisting collective levels, single-particle levels, and magnetic rotational bands [1–7]. For the indium isotopes, shape coexistence phenomena were reported in odd-A $^{107,111-117}$In [8–12] and possible magnetic rotational bands were also suggested in $^{107-114}$In [8,9,13–17] in the past two decades. It is of particular interest to investigate the systematic properties of these structure features to heavier indium nuclei. However, the excited states of In isotopes with $N \geqslant 66$ have not been studied extensively because of the relative difficulty in populating the high-spin states. High-spin states of ^{115}In were first studied via the fusion-evaporation reaction ^{100}Mo(^{18}O, p2n)^{115}In [11] in 1997. Later, Lucas *et al.* reported a more complete level scheme using the fusion-fission reaction ^{31}P + ^{176}Yb [12]. In Ref. [12], no angular correlation analysis was performed, and the spin-parity assignments were based on the empirical arguments or the analogy with the level structure of ^{113}In. It is worth mentioning that there exist some differences between the placement of transitions in Refs. [11,12]. In this report, we present the new experimental results of high-spin states in the $N = 66$ odd-A nucleus ^{115}In via the ^{114}Cd (^{7}Li, $\alpha 2n$) reaction and employ the tilted axis cranking model based on covariant density functional theory (TAC-CDFT) to analyze the level structure of ^{115}In.

II. EXPERIMENTAL PROCEDURE

The ^{115}In nucleus was produced in the ^{114}Cd(^{7}Li, $\alpha 2n$) fusion-evaporation reaction at a beam energy of 48 MeV. The beam was delivered by the HI-13 tandem accelerator at the China Institute of Atomic Energy in Beijing. A self-supporting target consisting of two stacked 2.5 mg/cm^2 metallic foils was used. The γ rays were detected using an array composed of 12 Compton-suppressed high-purity germanium (HPGe) bismuth germanate (BGO) detectors and two planar-type HPGe detectors. A total of 1.2×10^8 γ-γ coincidence events were recorded. The detailed experimental setup and procedure can be found in Ref. [5]. To profit from the full efficiency and cancel the restriction of the gate transition, two new asymmetric ADO (angular distribution from oriented states) [18] matrices were constructed using the γ rays detected at all angles (y axis) against those detected at $\sim$45° (or $\sim$135°) and $\sim$90° (x axis), respectively. This method is very useful for the near-spherical nucleus. In the present geometry, the ADO ratios of 1.1 and 0.8 are expected for the stretched quadrupole or $\Delta I = 0$ dipole radiations and pure dipole transitions, respectively.

III. RESULTS AND DISCUSSION

As already mentioned in the Introduction, there exist some differences between the placement of transitions in Refs. [11,12]. Based on the present γ-γ coincidence relations and γ-ray intensities, we confirm the transition placements of Ref. [12]. Moreover, 13 new transitions and 10 new levels are added into the level scheme of ^{115}In. Figure 1 gives examples of the gated γ-γ coincidence spectra. Most of the transitions assigned to ^{115}In can be seen in Fig. 1, where the new transitions are denoted by asterisks. Spin and parity assignments of all levels in ^{115}In were based on the present measured ADO ratios where possible, and spin/energy systematics where not. The ADO ratios of transitions, together with energies, intensities, and spin assignments are given in Table I. The level scheme of ^{115}In deduced from the present work is shown in Fig. 2, which is separated into three parts and labeled A–C for the convenience of discussion.

A. Structure A

Structure A of ^{115}In has been extended by adding two new levels and three new transitions in the present work. Moreover, the spin-parity of the state depopulated by the transition of

*Corresponding author: sywang@sdu.edu.cn

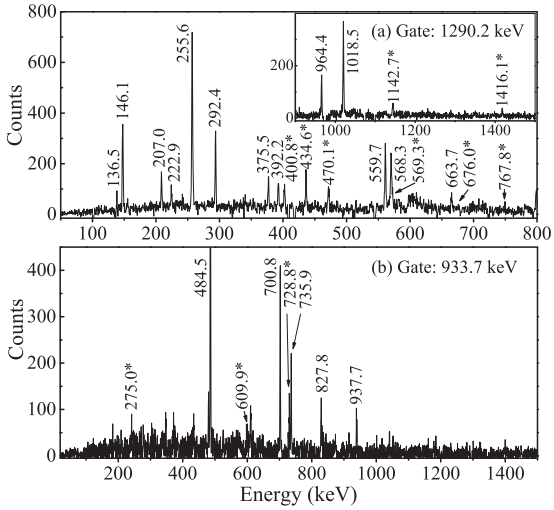

FIG. 1. Coincidence spectra obtained by gating on (a) the 1290.2-keV transition, and (b) the 933.7-keV transition. New transitions observed in the present work are denoted with asterisks.

937.7 keV has been modified from $(9/2^-)$ [19] to $(7/2^+)$ based on the measured ADO ratio and spin/energy systematics. As stated in Ref. [19], the spin-parity assignment of the $I^\pi = (9/2^-)$ state at 0.94 MeV was less reliable, with which the origin of this state was unclear. The present measured ADO ratio of 937.7 keV is 1.08(0.23), which indicated the character of stretched quadrupole or $\Delta I = 0$ dipole for the transition. We adopted the $\Delta I = 0$ dipole character for the 937.7 keV transition based on the following systematic comparison. A systematic correlation between the positive-parity states based on the $7/2_1^+$ state in ^{115}In and that based on the 0_1^+ state in ^{114}Cd [20] was illustrated in Fig. 3. Here the $7/2_1^+$ state of ^{115}In was designated as 0 in energy for the convenience of comparison. As shown in Fig. 3, there is a remarkable similarity between the states in ^{115}In and ^{114}Cd. These states in ^{115}In can be well described in terms of weakly coupling a $g_{7/2}$ proton to the ^{114}Cd core. Thus, the state depopulated by the 937.7 keV transition in ^{115}In could be interpreted as the $\pi g_{7/2} \otimes (^{114}\text{Cd}, 0_2^+)$ configuration, thereby supporting the $I^\pi = (7/2^+)$ assignment for this state. In view of the character of quadrupole vibration of the yrast states in the ^{114}Cd core [20], structure A of ^{115}In may be regarded as originating from the collective behavior.

B. Structure B

As compared with the recent work of Lucas *et al.* [12], we added a total of seven new levels and nine new transitions into structure B. In Ref. [12], no angular correlation analysis was performed, and the spin-parity assignments were based on the empirical arguments or the analogy with the level structure of ^{113}In. It should be noted that most of the spin-parity assignments in the present work are consistent with those of Ref. [12], except that spins and parities of the states depopulated by 559.7 and 964.4 keV transitions are modified as $(21/2^+)$ and $(13/2^+)$, respectively. In contrast to structure A, structure B displays rather irregular level structures,

TABLE I. γ-ray energies, relative intensities, spin-parity assignments, and measured ADO ratios for transitions assigned to ^{115}In.

E_γ (keV)	I_γ	$I_i^\pi \rightarrow I_f^\pi$	ADO ratio
82.0	14.2(3.6)	$(23/2^+) \rightarrow (21/2^+)$	
136.5	8.9(1.5)	$(25/2^+) \rightarrow (23/2^+)$	
146.1	22.0(0.2)	$(17/2^-) \rightarrow (15/2^-)$	
146.3	3.0(0.6)	$(25/2^-) \rightarrow (23/2^-)$	
157.8	<2	$13/2^+ \rightarrow 11/2^+$	
207.0	3.8(0.4)	$(23/2^-) \rightarrow (21/2^-)$	
222.9	5.0(0.8)	$(21/2^+) \rightarrow (17/2^+)$	0.89(0.19)
255.6	23.4(1.6)	$(19/2^-) \rightarrow (17/2^-)$	1.00(0.16)
275.0	<2	$(11/2^+) \rightarrow (7/2^+)$	
292.4	18.6(0.3)	$(21/2^-) \rightarrow (19/2^-)$	0.78(0.13)
336.8	<2	$(17/2^+) \rightarrow (17/2^+)$	
340.1	2.2(0.4)	$(21/2^+) \rightarrow (19/2^-)$	
375.5	5.4(0.9)	$(27/2^+) \rightarrow (25/2^+)$	0.69(0.11)
392.2	9.4(1.2)	$(17/2^+) \rightarrow (13/2^+)$	1.00(0.19)
400.8	3.6(0.7)	$(19/2^-) \rightarrow (17/2^-)$	0.70(0.21)
434.6	13.4(1.1)	$(17/2^-) \rightarrow (15/2^-)$	0.88(0.17)
470.1	2.5(0.3)	$(21/2^-) \rightarrow (19/2^-)$	
484.5	13.7(1.2)	$(11/2^+) \rightarrow 7/2^+$	1.24(0.09)
559.7	21.7(2.9)	$(21/2^+) \rightarrow (17/2^+)$	1.00(0.18)
568.3	13.9(1.7)	$(21/2^+) \rightarrow (17/2^+)$	1.20(0.24)
569.3	10.0(1.3)	$(17/2^+) \rightarrow (15/2^-)$	0.89(0.12)
569.4	~5	$(29/2^+) \rightarrow (27/2^+)$	
609.9	2.1(0.4)	$(23/2^+) \rightarrow (19/2^+)$	
663.7	<2	$(27/2^-) \rightarrow (25/2^-)$	
676.0	2.3(0.4)	$(31/2^+) \rightarrow (29/2^+)$	
700.8	7.0(0.2)	$(15/2^+) \rightarrow (11/2^+)$	1.18(0.18)
728.8	2.5(0.3)	$(11/2^+) \rightarrow (11/2^+)$	0.94(0.14)
735.9	<2	$(29/2^-) \rightarrow (27/2^-)$	
767.8	2.1(0.3)	$(21/2^+) \rightarrow (17/2^+)$	0.74(0.31)
827.8	4.2(0.6)	$(19/2^+) \rightarrow (15/2^+)$	1.27(0.23)
845.9	58.3(4.0)	$(15/2^-) \rightarrow 13/2^+$	0.80(0.12)
933.7	16.8(1.9)	$7/2^+ \rightarrow 9/2^+$	0.63(0.13)
937.7	3.3(0.5)	$(7/2^+) \rightarrow 7/2^+$	1.08(0.23)
964.4	9.7(1.5)	$(13/2^+) \rightarrow 13/2^+$	1.13(0.24)
1018.5	25.6(1.3)	$(17/2^+) \rightarrow 13/2^+$	0.92(0.17)
1132.3	<2	$11/2^+ \rightarrow 9/2^+$	
1142.7	3.7(0.4)	$(15/2^+) \rightarrow 13/2^+$	0.52(0.13)
1290.2	100.0	$13/2^+ \rightarrow 9/2^+$	1.10(0.09)
1398.4	<2	$(29/2^-) \rightarrow (25/2^-)$	
1416.1	3.0(0.5)	$(17/2^+) \rightarrow 13/2^+$	1.30(0.29)

which could be understood by coupling a $g_{9/2}$ proton hole to various ^{116}Sn core states. The systematic comparison of structure B with the corresponding states in the ^{116}Sn core nucleus [21,22] was performed and illustrated in Fig. 4. As exhibited in Fig. 4, states in structure B are close in energy to the corresponding core states in ^{116}Sn, which supports the description of $\pi(g_{9/2})^{-1} \otimes {}^{116}$Sn for structure B.

C. Structure C

Structure C has been extended up to $(31/2^+)$, which manifests itself as a rotational-like band with strong $M1$ transitions connecting the levels and no $E2$ crossover transitions. This dipole band has been suggested as the $\pi(g_{9/2})^{-1} \otimes \nu(h_{11/2})^2$

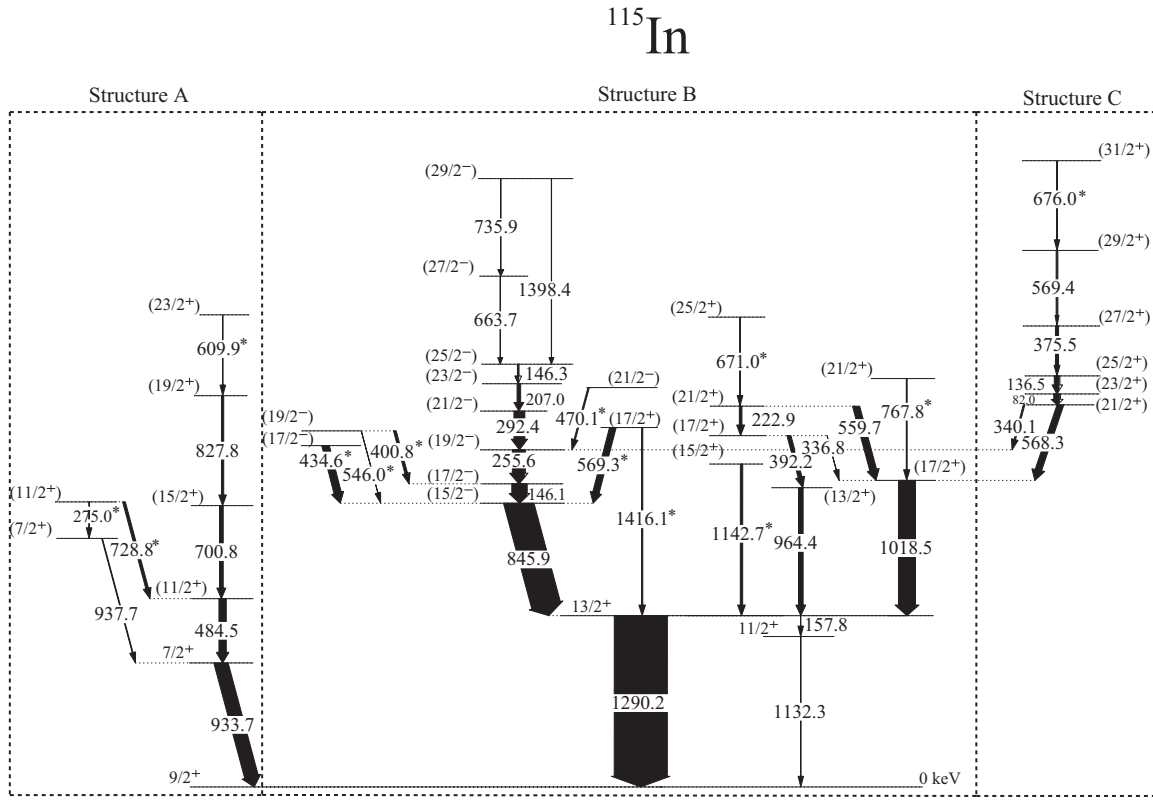

FIG. 2. Level scheme of ^{115}In. New transitions observed in the present work are denoted by asterisks.

configuration [12]. Similar three-quasiparticle bands have also been observed in lighter ^{111}In [9] and ^{113}In [10,16] nuclei, and tentatively interpreted as the magnetic rotational (MR) bands.

To obtain further insight into the structure C of ^{115}In, we performed the tilted axis cranking model based on covariant density functional theory (TAC-CDFT) calculations with the $\pi(g_{9/2})^{-1} \otimes \nu(h_{11/2})^2$ configuration. The TAC-CDFT with the point-coupling interaction was established in Ref. [23], which has succeeded in describing the MR in mass regions $A \sim 60$, 80, 100, 140, and 200 (see review [24] and references therein),

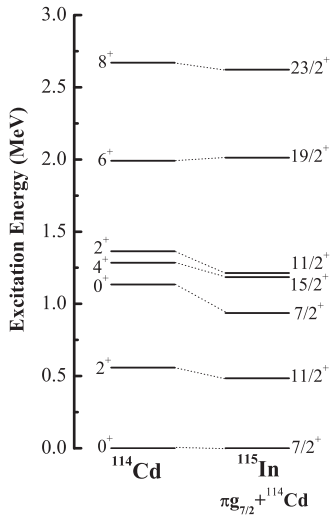

FIG. 3. Comparison of the positive-parity states based on the $7/2^+_1$ in ^{115}In with the corresponding states in the ^{114}Cd core nucleus [20].

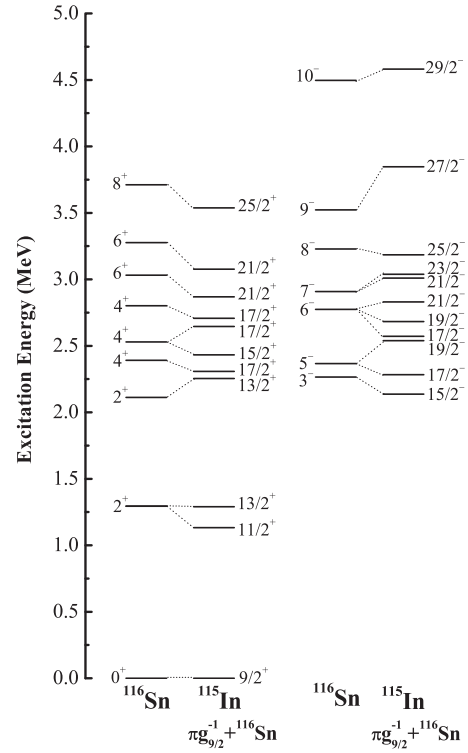

FIG. 4. Comparison of the states in structure B of ^{115}In with the corresponding states in the ^{116}Sn core nucleus [21,22].

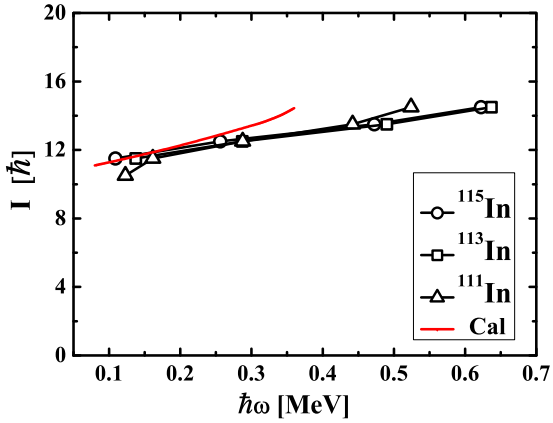

FIG. 5. (Color online) Total angular momentum as a function of the rotational frequency in the TAC-CDFT calculations for the structure C in ^{115}In are compared with the corresponding experimental data, together with the $\pi(g_{9/2})^{-1} \otimes \nu(h_{11/2})^2$ bands in ^{113}In [16] and ^{111}In [9].

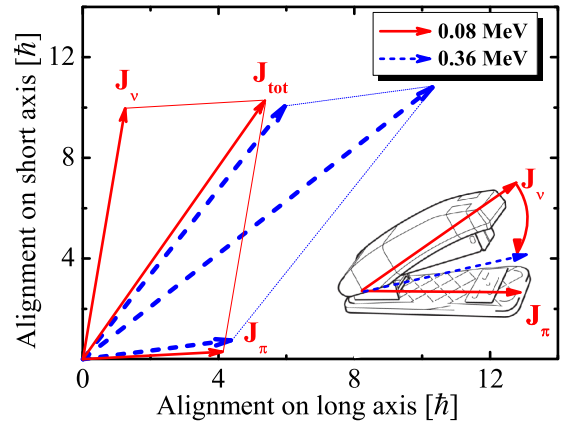

FIG. 6. (Color online) Compositions of the proton and neutron angular momentum vectors J_π and J_ν as well as the total angular momentum $J_{\rm tot} = J_\pi + J_\nu$ at both rotational frequencies of 0.08 and 0.36 MeV in the TAC-CDFT calculations with the $\pi(g_{9/2})^{-1} \otimes \nu(h_{11/2})^2$ configuration. The inset shows a schematic view of the stapler.

as well as antimagnetic rotation (AMR) in ^{105}Cd [25,26], ^{109}Cd [27], and ^{112}In [28]. In our TAC-CDFT calculations with parameter set PC-PK1 [29], a basis of eight major oscillator shells is adopted and pairing correlations are neglected. The calculated angular momenta as a function of rotational frequency for the structure C in ^{115}In are compared with the corresponding experimental values in Fig. 5, together with the $\pi(g_{9/2})^{-1} \otimes \nu(h_{11/2})^2$ bands in ^{111}In [9] and ^{113}In [16]. As shown in Fig. 5, the curve of the structure C in ^{115}In is very similar to those of ^{111}In and ^{113}In, and the calculated values to some extent are in agreement with the experimental results. It further supports the $\pi(g_{9/2})^{-1} \otimes \nu(h_{11/2})^2$ configuration assignment for structure C of ^{115}In.

To examine the possible MR mechanism of the $\pi(g_{9/2})^{-1} \otimes \nu(h_{11/2})^2$ band in ^{115}In, the proton and neutron angular momentum vectors J_π and J_ν as well as the total angular momentum $J_{\rm tot} = J_\pi + J_\nu$ at both rotational frequencies of 0.08 and 0.36 MeV are calculated and illustrated in Fig. 6. Here, the J_π (J_ν) is the sum of all the proton (neutron) orbitals occupied in the cranking wave function. For the MR band, the angular momentum vectors for both protons and neutrons are almost perpendicular at the bandhead, which move toward each other to the direction of the total angular momentum as the rotational frequency increases while the direction of the total angular momentum is nearly invariant. The major part of the total angular momentum is gained by a gradual alignment of the individual proton and neutron spins into the direction of the total angular momentum. Only a small component of the total angular momentum is from collective rotation. This process resembles the closing of the blades of a pair of shears, so also called "shear band" [30]. As shown in Fig. 6, with the frequency increases, the only J_ν moves obviously toward the direction of the total angular momentum while J_π is almost motionless and then the tilted angles of the total angular momentum have an obvious change. This behavior is not identical to the simultaneous closing of the blades of a pair of shears, but similar to the closing of a stapler (see the inset of Fig. 6). Therefore, we suggest the term "stapler bands" for these structures. It is worthwhile mentioning that the recent TAC-CDFT calculations for the $N = 79$ isotones in the $A \sim 140$ mass region [31] also exhibited a similar picture of the stapler closing. It also indicates that the stapler bands could be of a general nature and not only related to a specific nuclear region.

The magnetic and electric rotations are two extreme cases that can be well distinguished. The stapler mechanism suggested in the present work should be expected to be the intermediate situation where both types of rotation compete. The total angular momentum gain may then contain contributions from the shears mechanism and from the rotation of the core. Therefore, it is very interesting to study the competition between the shears mechanism and core rotation in the stapler band. However, in the TAC-CDFT calculations, $J_{\rm tot} = J_\pi + J_\nu$ and there is no inert core. To investigate the proportion of the two modes in angular momentum generation, we used a simple picture to define MR and core angular momentum. The angular momentum increment coming from $\pi(g_{9/2})^{-1}$ and $\nu(h_{11/2})^2$ is defined as the contribution of the two-shears mechanism. The core angular momentum is defined by excluding the contributions of valence nucleons from the total angular momentum. Thus,

$$\begin{aligned} \Delta J_{\rm tot} &= \Delta j_{\pi g_{9/2}^{-1}} + \Delta j_{\nu h_{11/2}^2} + \Delta J_{\rm core} \\ &= \Delta J_{\rm shear} + \Delta J_{\rm core}. \end{aligned} \quad (1)$$

By this approach, $\Delta J_{\rm shear} : \Delta J_{\rm core}$ is approximate to 4 : 6 when the rotational frequency increases from 0.08 to 0.36 MeV. It indicates there exist the strong competition between the shears mechanism and collective rotation, and the collective rotation of the core plays a more dominant role than the shears mechanism in the structure C of ^{115}In.

The evolutions of deformation parameters β_2 and γ for the $\pi(g_{9/2})^{-1} \otimes \nu(h_{11/2})^2$ band of ^{115}In are calculated and displayed in Fig. 7 with the rotational frequency increasing from 0.08 to 0.36 MeV. As shown in Fig. 7, the calculated β_2 values are about 0.15 and the γ values are about 50°.

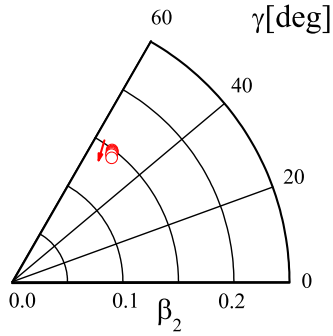

FIG. 7. (Color online) Evolutions of deformation parameters β_2 and γ driven by increasing rotational frequency in the TAC-CDFT calculations for structure C. The rotational frequencies increase from 0.08 to 0.36 MeV for the $\pi(g_{9/2})^{-1} \otimes \nu(h_{11/2})^2$ configuration.

Consequently, the small oblate deformation for structure C is clearly exhibited. With these features in mind, we propose the structure C of ^{115}In as an oblate band built on the "stapler mechanism." It should be noted that for the oblate band C, the core rotation grows along the long axis, which will lead to a gradual alignment of the proton and neutron spins into the long axis. In Fig. 6, the direction of J_π is almost parallel to the long axis at the bandhead, so that it may keep near invariability with the frequency increases. Based on the discussion above, we propose that the "stapler band" can be formed if the direction of J_π (J_ν) is almost parallel to the growing direction of collective rotation in the nucleus in which exists strong competition between the shear mechanism and collective rotation.

IV. SUMMARY

In summary, high-spin states of ^{115}In were studied using the ^{114}Cd (^{7}Li, $\alpha 2n$) fusion-evaporation reaction at a beam energy of 48 MeV. A total of 10 new levels and 13 new transitions have been added to the level scheme of ^{115}In. Most of the states in ^{115}In can be interpreted in terms of weak coupling of a $g_{9/2}$ proton hole to the core states of ^{116}Sn and a $g_{7/2}$ proton to the core states of ^{114}Cd. The previously known dipole band with the $\pi(g_{9/2})^{-1} \otimes \nu(h_{11/2})^2$ configuration has been extended. The TAC-CDFT calculations suggest this band is a stapler band with the oblate deformation.

ACKNOWLEDGMENTS

This study is supported by the National Natural Science Foundation (Grants No. 11175108 and No. 11005069), the Independent Innovation Foundation of Shandong University IIFSDU (No. 2013ZRYQ001), and the National Undergraduate Innovative and Entrepreneurship Training Program of Shandong University at WeiHai (No. 201210422096) of China. The computations were carried out on an HP Proliant DL785G6 server hosted by the Institute of Space Science of Shandong University.

[1] K. Heyde, P. Van Isacker, M. Waroquier, J. L. Wood, and R. A. Meyer, Phys. Rep. **102**, 291 (1983).
[2] K. Heyde and J. L. Wood, Rev. Mod. Phys. **83**, 1467 (2011).
[3] S. Y. Wang *et al.*, Phys. Rev. C **81**, 017301 (2010).
[4] S. Y. Wang *et al.*, Phys. Rev. C **82**, 057303 (2010).
[5] S. Y. Wang *et al.*, Phys. Rev. C **86**, 064302 (2012).
[6] L. Liu *et al.*, Phys. Rev. C **90**, 014313 (2014).
[7] R. M. Clark and A. O. Macchiavelli, Annu. Rev. Nucl. Part. Sci. **50**, 1 (2000).
[8] D. Negi *et al.*, Phys. Rev. C **81**, 054322 (2010).
[9] P. Vaska, D. B. Fossan, D. R. LaFosse, H. Schnare, M. P. Waring, S. M. Mullins, G. Hackman, D. Prévost, J. C. Waddington, V. P. Janzen, D. Ward, R. Wadsworth, and E. S. Paul, Phys. Rev. C **57**, 1634 (1998).
[10] R. S. Chakrawarthy and R. G. Pillay, Phys. Rev. C **55**, 155 (1997).
[11] S. Naguleswaran *et al.*, Z. Phys. **359**, 235 (1997).
[12] R. Lucas *et al.*, Eur. Phys. J. A **15**, 315 (2002).
[13] C. J. Chiara *et al.*, Phys. Rev. C **64**, 054314 (2001).
[14] D. Negi *et al.*, Phys. Rev. C **85**, 057301 (2012).
[15] C. Y. He *et al.*, Phys. Rev. C **83**, 024309 (2011).
[16] K. Y. Ma *et al.*, Eur. Phys. J. A **48**, 82 (2012).
[17] C. B. Li *et al.*, Nucl. Phys. A **892**, 34 (2012).
[18] M. Piiparinen *et al.*, Nucl. Phys. A **605**, 191 (1996).
[19] A. B. Smith *et al.*, J. Phys. G **11**, 125 (1985).
[20] S. Juutinen *et al.*, Phys. Lett. B **386**, 80 (1996).
[21] A. Savelius *et al.*, Nucl. Phys. A **637**, 491 (1998).
[22] Jean Blachot, Nucl. Data. Sheet **111**, 717 (2010).
[23] P. W. Zhao, S. Q. Zhang, J. Peng, H. Z. Liang, P. Ring, and J. Meng, Phys. Lett. B **699**, 181 (2011).
[24] J. Meng, J. Peng, S. Q. Zhang, and P. W. Zhao, Front. Phys. **8**, 55 (2013).
[25] P. W. Zhao, J. Peng, H. Z. Liang, P. Ring, and J. Meng, Phys. Rev. Lett. **107**, 122501 (2011).
[26] P. W. Zhao, J. Peng, H. Z. Liang, P. Ring, and J. Meng, Phys. Rev. C **85**, 054310 (2012).
[27] P. Zhang, B. Qi, and S. Y. Wang, Phys. Rev. C **89**, 047302 (2014).
[28] X. W. Li *et al.*, Phys. Rev. C **86**, 057305 (2012).
[29] P. W. Zhao, Z. P. Li, J. M. Yao, and J. Meng, Phys. Rev. C **82**, 054319 (2010).
[30] S. Frauendorf, Rev. Mod. Phys. **73**, 463 (2001).
[31] Y. Y. Cheng *et al.*, Phys. Rev. C **89**, 054309 (2014).